Stator-Flux-Oriented Vector Control of Synchronous Reluctance Machines With Maximized Efficiency

Heath F. Hofmann, *Member, IEEE*, Seth R. Sanders, *Member, IEEE*, and Ahmed EL-Antably, *Member, IEEE*

***Abstract*—This paper presents a position-sensorless vector torque controller designed to achieve maximum efficiency over a range of power and rotational speed for a synchronous reluctance machine. A model of the synchronous reluctance machine is presented which incorporates both winding and core losses. It is then shown that a stator-flux-oriented control scheme can achieve synchronous operation of the machine without a position sensor at medium and high electrical frequencies. For a given speed and torque, power losses in the machine are shown to be a function of only the stator flux magnitude. As the power losses are a convex function of the stator flux level, the optimal flux value can be found using a one-dimensional optimization algorithm, such as the Method of Sequential Quadratic Interpolations. Optimal flux values for a synchronous reluctance machine are determined using an experimental setup that accurately determines losses in the motor/drive system. Experimental results obtained from the test setup confirm the validity of the controller and the optimization algorithm.**

***Index Terms*—Field-oriented control (FOC), optimal control, synchronous reluctance machine.**

I. Introduction

SYNCHRONOUS reluctance machines have been shown to be an attractive alternative to induction and permanent-magnet machines in certain variable-speed drive applications. These machines have torque and efficiencies which are similar to those of induction machines [15], but with significantly lower rotor losses. These machines can also be designed with robust rotor structures which allow extremely high operational speeds [3]. Furthermore, the ability to regulate the flux levels in these machines and, hence, eliminate "spinning" core losses, can make these machines preferable to permanent-magnet machines in applications where the machine spends much of its time spinning without torque. One application which utilizes many of the above-mentioned advantages is a motor/generator for a flywheel energy storage system [4].

Vector control of synchronous reluctance machines typically requires some form of position feedback. However, the addition of a position sensor can be difficult, can reduce the reliability of the controller, and can incur prohibitive expense in many applications, particularly those which operate the machine at high speed. A position-sensorless torque control scheme for these machines is, therefore, highly desirable. It is also desirable to operate the machine at the operating point which maximizes the efficiency of the machine for a given torque and speed [10], [5], [9]. In this paper, we present a stator-flux-oriented control scheme which has both of these attributes. As the presented control scheme regulates the stator flux magnitude and torque it is similar to torque vector control [7], but the implementation presented here uses standard field-oriented control (FOC) techniques. The paper begins by presenting a machine model for the synchronous reluctance machine which incorporates winding and core losses [14], [16], [8], [2]. It is shown that the losses of the machine for a given speed and torque are solely a function of stator flux magnitude. The machine dynamics in the stator flux reference frame are then derived. Next, we present a position-sensorless stator-flux-oriented control scheme which can maintain synchronism at medium and high electrical frequencies. A method of determining maximum-efficiency operating points using an iterative search routine is developed. Finally, experimental results are presented.

TABLE I
Parameters and Ratings of Synchronous Reluctance Machine

No. Pole-Pairs (P)	1
Direct Inductance (L_d)	$1.93mH$
Quadrature Inductance (L_q)	$0.27mH$
DC Winding Resistance (R)	$44.5m\Omega$
Core Loss Conductance (G_c)	$0.154\Omega^{-1}$
Rated Flux Linkage ($\|\lambda\|$)	$0.15Wb_{pk}$
Rated Current ($\|\mathbf{i}\|$)	$150A_{pk}$

II. Machine Model

In this paper, all data presented will be based upon a synchronous reluctance machine designed at the University of California at Berkeley. The parameters and ratings of this machine are presented in Table I. Machine parameters were estimated from experimental data taken at several different operating points using a least-squares approach. Details of the machine design can be found in [4].

In the following, electrical variables of the machine will be presented in two-phase vector form, e.g.,

$$\mathbf{i} = \begin{bmatrix} i_\alpha \\ i_\beta \end{bmatrix}. \tag{1}$$

A two-phase lumped-parameter model of the synchronous reluctance machine is shown in Fig. 1. Due to the salient nature of

Manuscript received November 14, 2001; revised February 7, 2003. Abstract published on the Internet July 15, 2004. This paper was presented at the 20th International Telecommunications Energy Conference, San Francisco, CA, October 4–8, 1998.

H. F. Hofmann is with the Department of Electrical Engineering, The Pennsylvania State University, University Park, PA 16802 USA (e-mail: hofmann@ee.psu.edu).

S. R. Sanders is with the Department of Electrical Engineering and Computer Sciences, University of California, Berkeley, CA 94720 USA.

A. EL-Antably is with Allison Transmission, Indianapolis, IN 46250 USA.

Digital Object Identifier 10.1109/TIE.2004.834968

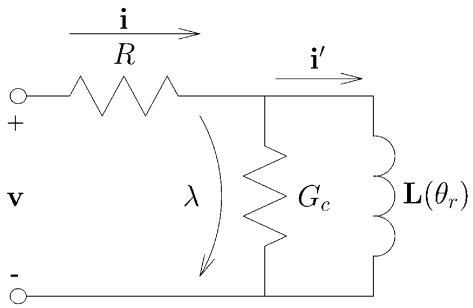

Fig. 1. Two-phase lumped-parameter model of stator windings of synchronous reluctance machine.

the rotor of a synchronous reluctance machine, the inductance $\mathbf{L}(\theta_r)$ has a two-phase matrix representation

$$\mathbf{L}(\theta_r) = e^{\mathbf{J}P\theta_r}\mathbf{L}e^{-\mathbf{J}P\theta_r} \tag{2}$$

where

$$\mathbf{J} = \begin{bmatrix} 0 & -1 \\ 1 & 0 \end{bmatrix} \quad \mathbf{L} = \begin{bmatrix} L_d & 0 \\ 0 & L_q \end{bmatrix} \tag{3}$$

P is the number of pole-pairs of the machine, and θ_r is the angular position of the rotor with respect to the stator.

The instantaneous electromagnetic torque produced by the machine is derived in Appendix A, and is given by

$$\tau_e = \frac{3P}{2}(\mathbf{i} - G_c\mathbf{v})^T\mathbf{J}\lambda. \tag{4}$$

The $G_c\mathbf{v}$ term in the expression above can be thought of as a "drag" torque generated by resistance to the changing magnetic fields in the stator iron.

The two-phase electrical dynamic equations are given in the stationary reference frame by

$$\frac{d}{dt}\lambda = -R\mathbf{i} + \mathbf{v}. \tag{5}$$

The input to the machine is considered to be the stator voltage, with the stator current as output. The expression for the stator current as a function of flux-linkage and stator voltage is derived as follows:

$$\begin{aligned} \lambda = \mathbf{L}(\theta_r)\mathbf{i}' = \mathbf{L}(\theta_r)[\mathbf{i} - G_c(\mathbf{v} - R\mathbf{i})] \\ \Rightarrow \mathbf{i} = (1 + G_cR)^{-1}[\mathbf{L}^{-1}(\theta_r)\lambda + G_c\mathbf{v}]. \end{aligned} \tag{6}$$

III. Stator-Flux Orientation

In the following, we present a stator-flux-oriented torque control scheme. Electrical variables are transformed into the flux reference frame using the Park transformation

$$\mathbf{x}^\lambda = e^{-\mathbf{J}\rho}\mathbf{x} \tag{7}$$

where ρ represents the instantaneous electrical angle between the flux vector and the stationary reference frame

$$\rho = \tan^{-1}\left(\frac{\lambda_\beta}{\lambda_\alpha}\right). \tag{8}$$

In the flux reference frame $\lambda_d^\lambda = \|\lambda\|$, or the flux magnitude, and $\dot{\lambda}_q^\lambda = \lambda_q^\lambda = 0$. The dynamic equations in this reference frame can be shown to be

$$\frac{d}{dt}\begin{bmatrix} \|\lambda\| \\ 0 \end{bmatrix} = -\omega_e\mathbf{J}\begin{bmatrix} \|\lambda\| \\ 0 \end{bmatrix} - R\begin{bmatrix} i_d^\lambda \\ i_q^\lambda \end{bmatrix} + \begin{bmatrix} v_d^\lambda \\ v_q^\lambda \end{bmatrix} \tag{9}$$

$$\mathbf{i}^\lambda = (1 + G_cR)^{-1}(e^{\mathbf{J}\theta_s}\mathbf{L}^{-1}e^{-\mathbf{J}\theta_s}\lambda + G_c\mathbf{v}^\lambda) \tag{10}$$

$$\theta_s = \rho - P\theta_r \tag{11}$$

where $\omega_e = \dot{\rho}$ is the instantaneous angular velocity of the rotating flux vector and θ_s is the electrical angle between the flux reference frame and the rotor's direct axis. Note that in steady-state operation the angle θ_s is constant.

From (9) we can derive an expression for ω_e

$$\omega_e = \frac{v_q^\lambda - Ri_q^\lambda}{\|\lambda\|}. \tag{12}$$

The dynamics of θ_s are, therefore, given by

$$\frac{d}{dt}\theta_s = \omega_e - P\omega_r = \frac{v_q^\lambda - Ri_q^\lambda}{\|\lambda\|} - P\omega_r \tag{13}$$

and the stator flux dynamics reduce to

$$\frac{d}{dt}\|\lambda\| = -Ri_d^\lambda + v_d^\lambda. \tag{14}$$

The stator current vector in this reference frame is given by

$$\mathbf{i}^\lambda = (1 + G_cR)^{-1}(e^{-\mathbf{J}\theta_s}\mathbf{L}^{-1}e^{\mathbf{J}\theta_s}\lambda^\lambda + G_c\mathbf{v}^\lambda). \tag{15}$$

Under steady-state conditions the stator voltage can be written as

$$\begin{aligned} v_d^\lambda &= Ri_d^\lambda, \\ v_q^\lambda &= Ri_q^\lambda + \omega_e\|\lambda\|. \end{aligned} \tag{16}$$

Substitution of (16) into (15) yields an expression for steady-state stator current

$$\mathbf{i}^\lambda = \begin{bmatrix} \left(\frac{1}{L_q} + \frac{1}{L_d}\right) - \left(\frac{1}{L_q} - \frac{1}{L_d}\right)\cos 2\theta_s \\ \left(\frac{1}{L_q} - \frac{1}{L_d}\right)\sin 2\theta_s + 2G_c\omega_e \end{bmatrix} \frac{\|\lambda\|}{2}. \tag{17}$$

A plot of (17), parameterized by θ_s, is shown in Fig. 2. As can be seen in the figure, the core loss is represented by an offset of the stator current locus in the quadrature direction. This offset can be compensated for by adding a $G_c\omega_e\|\lambda\|$ term to the quadrature current in order to obtain more accurate torque calculation and control.

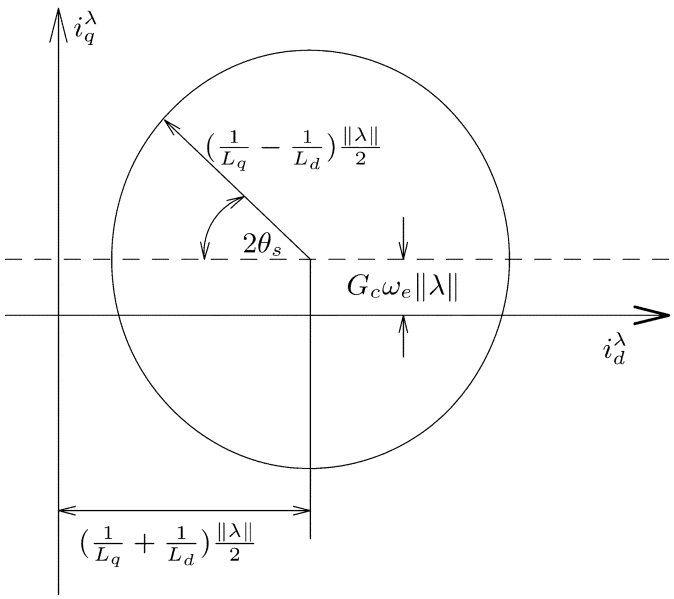

Fig. 2. Stator current locus in stator-flux reference frame.

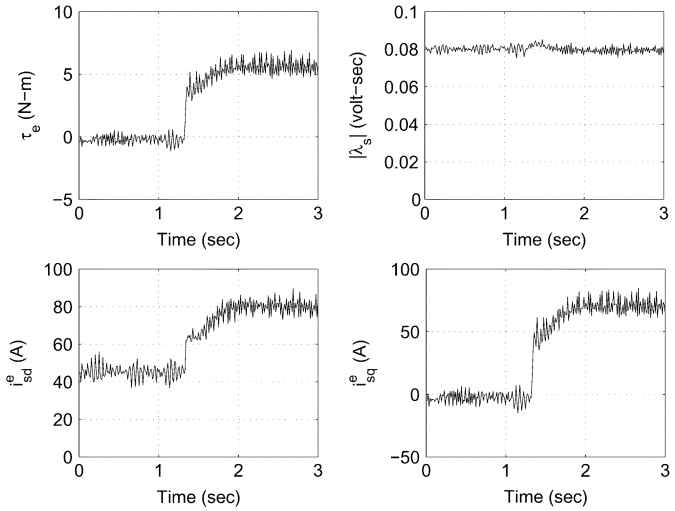

Fig. 3. Torque step from 0 to 6 N·m. $\|\bar{\lambda}\| = 0.08$ Wb. Plots, going clockwise from top left, are electrical torque, stator flux magnitude, and quadrature and direct stator currents.

IV. Control Scheme

The torque expression in (32) is invariant with respect to reference frame and, hence, $\tau_e = (3P/2)\mathbf{i}'^T\mathbf{J}\lambda = (3P/2)\|\lambda\|(i_q^\lambda - G_c v_q^\lambda)$. As G_c is frequency dependent and difficult to determine, in the following this component is neglected. We note, however, that this results in an error between the commanded torque and actual shaft torque.

Torque can, therefore, be controlled by regulating $\|\lambda\|$ and i_q^λ. Inspection of (14) suggests that a simple proportional–integral (PI) approach plus resistive drop compensation suffices to control $\|\lambda\|$ using v_d^λ

$$v_d^\lambda = Ri_d^\lambda + K_{p\lambda}(\|\tilde{\lambda}\| - \|\lambda\|) + K_{i\lambda}\int(\|\tilde{\lambda}\| - \|\lambda\|)\,dt. \quad (18)$$

Though the dynamics are not quite as straightforward, it can be shown that the quadrature stator current i_q^λ can be regulated using v_q^λ. A PI approach plus resistive drop compensation is also effective for this

$$\begin{aligned} v_q^\lambda &= Ri_q^\lambda + K_{pi}\left(\tilde{i}_q^\lambda - i_q^\lambda\right) + K_{ii}\int\left(\tilde{i}_{sq}^e - i_{sq}^e\right)dt \\ &= Ri_q^\lambda + \bar{v}_q^\lambda \end{aligned} \quad (19)$$

where $\bar{v}_q^\lambda$ is defined as the quadrature voltage after subtracting resistive drop, and is used in the following to simplify analysis.

The electrical dynamics of the quadrature current in this reference frame are nonlinear, so to facilitate analysis we derive the linearized transfer function between i_q^λ and $\bar{v}_q^\lambda$. This is obtained by linearizing the system at an operating point, characterized by $\|\lambda\|$ and θ_s. In this analysis the flux magnitude is assumed to be regulated to a constant value, and mechanical dynamics are neglected. That said, the transfer function is as follows:

$$\frac{I_q^\lambda(s)}{\bar{V}_q^\lambda(s)} = \frac{1}{s}\left(\frac{1}{L_q} - \frac{1}{L_d}\right)(\cos^2(\theta_s) - \sin^2(\theta_s)). \quad (20)$$

The derivation of this transfer function is presented in Appendix B. Inspection of (38) reveals that the gain of the transfer function changes sign when $\theta_s = \pm 45°$. Inspection of (17) and Fig. 3 reveals that, for a given $\|\lambda\|, i_q^\lambda$ reaches its maximum magnitude when $\theta_s = \pm 45°$

$$i_{q\max}^\lambda = \left[\frac{1}{2}\left(\frac{1}{L_q} - \frac{1}{L_d}\right) + G_c\omega_e\right]\|\lambda\|. \quad (21)$$

We note that $i_{q\max}^\lambda$ corresponds to the maximum torque achievable by the machine for a given stator flux magnitude. Hence, by commanding values of i_q^λ to be less than $i_{q\max}^\lambda$, we can avoid the change in sign of the transfer function. Another attractive feature of the above controller is that it is not directly dependent on values of the direct and quadrature inductances. As a result, it is anticipated that the controller will still work well even when the machine is magnetically saturated.

In our experimental setup, the three-phase voltages and currents from the machine are measured and converted into two-phase signals using analog circuitry. These signals are then sampled for use in the digital controller, a 90-MHz Pentium PC. The PC was able to control the machine with a time step of 140 μs. The two-phase stator flux is estimated in the controller by numerically integrating the two-phase stator voltage minus estimated resistive drop, with a decay term inserted to avoid numerical drift

$$\begin{aligned} \frac{d}{dt}\hat{\lambda}_\alpha &= -Ri_\alpha + v_\alpha - K\hat{\lambda}_\alpha \\ \frac{d}{dt}\hat{\lambda}_\beta &= -Ri_\beta + v_\beta - K\hat{\lambda}_\beta. \end{aligned} \quad (22)$$

The decay constant limits the operation of this controller to medium and high electrical frequencies.

Fig. 3 shows the results of a commanded torque step with the experimental setup using the flux-oriented controller. The electrical torque τ_e in the figure is determined by the cross product of measured stator current and estimated stator flux. The PI constants used in this experiment were $K_{p\lambda} = 200$, $K_{i\lambda} = 200$, $K_{pi} = 0.3$, and $K_{ii} = 10$. Bandwidths for the control

are 200 rad/s for the stator flux and approximately 700 rad/s for the quadrature stator current. The stator-flux-oriented controller is shown to work well, and is used in all of the following experiments.

V. Losses

In the model discussed in the prequel it is assumed that losses in the machine can be divided into two components; those proportional to the square of the magnitude of the winding currents, represented by the scalar "winding resistance" R

$$P_{Cu} = \frac{3}{2} R \|\mathbf{i}\|^2 \tag{23}$$

and those proportional to the square of the electromotive force magnitude, represented by the "core loss conductance" G_c, which are approximated with the expression

$$P_{\text{core}} = \frac{3}{2} G_c \omega_e^2 \|\lambda\|^2 \tag{24}$$

where ω_e is the electrical frequency.

Operating points typically discussed for the synchronous reluctance machine to achieve a given torque are the minimum current operating point, the minimum flux-linkage operating point, and the maximum power factor operating point [9]. These operating points could be chosen for varying reasons dependent upon the rotational speed of the machine. For example, operation near the minimum current operating point may be desirable at low speeds where it is desired that power output be maximized subject to current limitations of the power electronics inverter, and also because losses at low speeds are dominated by copper losses. Likewise, operation near the minimum flux-linkage operating point may be desirable at high speeds where the voltage limitations of the inverter constrains power output, and also because core losses may be significant. For a given torque and speed, it can be shown that there exists an optimal stator flux magnitude which minimizes losses that does not necessarily correspond to any of these operating points. Fig. 4 presents estimated copper and core losses of the synchronous reluctance machine at an 18-N·m 4000-r/min operating point over a range of flux magnitudes. Note that this model predicts a convex loss function, and that the optimal flux value is significantly different from the "conventional" operating points. Determining the optimal operating point from a machine model is not necessarily a robust approach, as the actual machine losses can deviate significantly from those predicted by the model. For example, saturation of the machine magnetics will affect the equivalent direct and quadrature inductances, thus changing the optimal operating points of the machine. Furthermore, the loss parameters of the machine tend to be significantly dependent upon frequency. The winding resistance R will increase with electrical frequency due to the skin and proximity effects, which decrease the effective cross-sectional area of the windings of the machine, and is therefore not constant as the model implies. Furthermore, a constant core loss conductance implies that core losses in the machine are proportional to the square of the electrical frequency for a given flux linkage magnitude. Losses in ferromagnetic materials are actually much more complex, with hysteresis losses being roughly proportional to electrical frequency and eddy current losses increasing more quickly with frequency, and so the core loss conductance must be considered to be frequency dependent as well. Because of the complicated frequency dependence of losses, it is difficult to accurately compute losses for the machine over a wide speed range. It is therefore preferable to determine optimal operating points for a given machine design through experimentation.

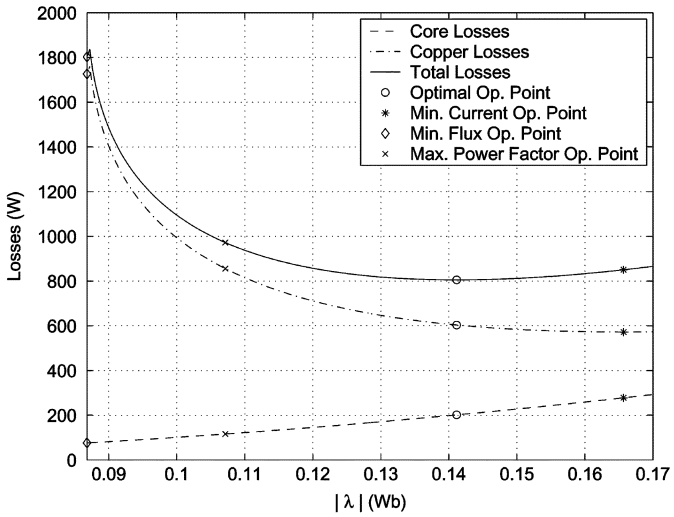

Fig. 4. Estimated synchronous reluctance machine losses over a range of stator flux levels. 18 N·m, 4000-r/min operating point.

VI. Optimal Controller

In order to determine the optimal flux level for a given operating point a variant of Newton's method, known as the Method of Sequential Quadratic Interpolations, is used [12], [6]. The method works as follows. The iterative process begins by driving the machine at a constant torque and speed in an experimental setup, discussed in detail in the following, using three different, strategically chosen flux magnitudes $\|\lambda\|_1, \|\lambda\|_2$, and $\|\lambda\|_3$. Care must be taken to ensure that only flux values sufficiently large to achieve the desired torque are allowed. For each flux value, the power flowing into the experimental setup, denoted $P_{\text{loss}\,1}, P_{\text{loss}\,2}$, and $P_{\text{loss}\,3}$ respectively, is measured. These three data points are then fit to a quadratic curve

$$P_{\text{loss}}(\|\lambda\|) = a\|\lambda\|^2 + b\|\lambda\| + c, \tag{25}$$

$$\begin{bmatrix} a \\ b \\ c \end{bmatrix} = \begin{bmatrix} \|\lambda\|_1^2 & \|\lambda\|_1 & 1 \\ \|\lambda\|_2^2 & \|\lambda\|_2 & 1 \\ \|\lambda\|_3^2 & \|\lambda\|_3 & 1 \end{bmatrix}^{-1} \begin{bmatrix} P_{\text{loss}\,1} \\ P_{\text{loss}\,2} \\ P_{\text{loss}\,3} \end{bmatrix}. \tag{26}$$

Supposing the loss is quadratic, we then estimate the stator flux which minimizes loss, according to the fitted curve

$$\|\lambda\|_{\text{opt}}^{(1)} = \frac{-b}{2a}. \tag{27}$$

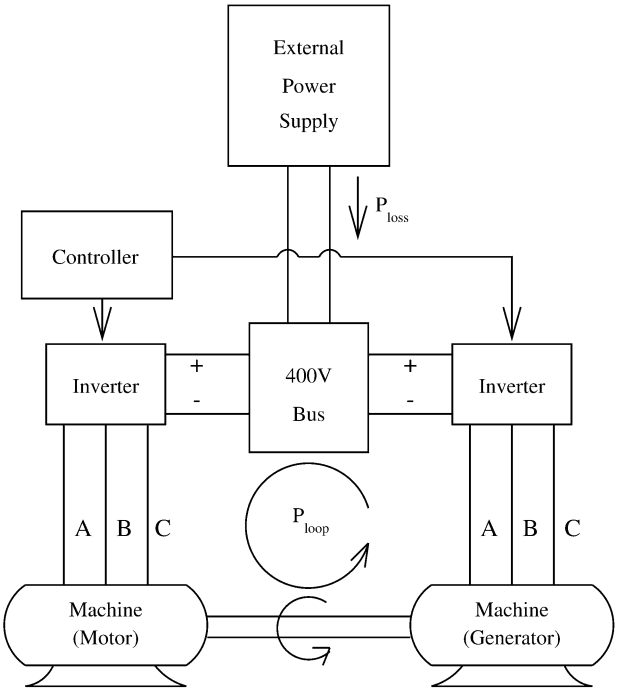

Fig. 5. Experimental setup.

By combining (26) and (27), the optimal flux expression becomes

$$\|\lambda\|_{\text{opt}}^{(1)} = \frac{d_1 s_1 P_{\text{loss}\,1} + d_2 s_2 P_{\text{loss}\,2} + d_3 s_3 P_{\text{loss}\,3}}{2(d_1 P_{\text{loss}\,1} + d_2 P_{\text{loss}\,2} + d_3 P_{\text{loss}\,3})},$$
$$d_1 = \|\lambda\|_3 - \|\lambda\|_2;$$
$$d_2 = \|\lambda\|_1 - \|\lambda\|_3;$$
$$d_3 = \|\lambda\|_2 - \|\lambda\|_1;$$
$$s_1 = \|\lambda\|_3 + \|\lambda\|_2;$$
$$s_2 = \|\lambda\|_1 + \|\lambda\|_3;$$
$$s_3 = \|\lambda\|_2 + \|\lambda\|_1. \tag{28}$$

The actual loss function of the machine is not a quadratic, and so an iterative approach must be taken to converge to the optimal value. This new value, along with two of the previous flux values, are used to reiterate the process. As will be shown, only a few iterations are needed to achieve adequate convergence. This algorithm, known as the Luenberger Sequential Quadratic Interpolations Algorithm, is guaranteed to converge to the optimal operating point provided the loss function is continuously differentiable and convex, as has been shown in [12].

A. Implementation

The experimental setup used is shown in Fig. 5. In this setup two identical synchronous reluctance machines are connected at the shaft. The machines are driven by identical 400-V 200-A inverters with *LC* output filters, which are connected to a common dc-voltage bus. Driving one machine as a motor and the other as a generator causes power to flow in a loop, from voltage bus to inverter to motor to generator to inverter and back to the voltage bus. An external power source is used to supply the necessary power to keep the machines at a given steady-state operating point. This dc input power, P_{loss}, corresponds to the total losses of the system and, hence, can be used to accurately determine the system efficiency. We note that this total loss includes inverter loss as well as machine loss and, hence, the proposed approach attempts to optimize the overall efficiency of the drive.

TABLE II
EXPERIMENTAL RESULTS OF OPTIMIZATION ALGORITHM, 8 N·m, 4 000-r/min OPERATING POINT

	Flux Level $\|\lambda\|$	P_{loss}
1st	$0.0911Wb$	$4,173W$
3 Flux	$0.1060Wb$	$3,588W$
Levels	$0.1260Wb$	$3,535W$
1st Estimated Optimal Flux	$0.1172Wb$	$3,427W$
2nd Estimated Optimal Flux	$0.1170Wb$	converged

The desired operating point is achieved by controlling torque on one machine and speed on the other. Speed is controlled through an outer speed PI control loop on the torque control of the machine. By commanding the same flux magnitude to both machines, and as the machines have approximately equal and opposite torque levels, the current magnitudes in the machines are roughly equivalent and, hence, power losses are approximately balanced between the two machines.

Table II shows results of an experiment where the optimization algorithm presented in (26) and (27) was applied at a 16-N·m 4000-r/min operating point. The algorithm is seen to converge after only two iterations.

This method is then used to determine the optimal flux magnitudes for a number of speed and power values on a grid. While ideally the optimal stator flux magnitude with no output power should be zero, there must be some small value commanded so that the controller can maintain operation. When the actual controller is implemented, optimal stator flux commands are interpolated for operating points which are not on the gridpoints. The approximate optimal flux value in a square element bounded by $\omega_i, \omega_{i+1}, P_j$, and P_{j+1} can be calculated using the following interpolation scheme:

$$\begin{aligned}\hat{\lambda}(\omega, P) = \frac{1}{\Delta\omega_i \Delta P_j}[&\hat{\lambda}_{i,j}(\omega_{i+1} - \omega)(P_{j+1} - P) \\ &+ \hat{\lambda}_{i+1,j}(\omega - \omega_i)(P_{j+1} - P) \\ &+ \hat{\lambda}_{i,j+1}(\omega_{i+1} - \omega)(P - P_j) \\ &+ \hat{\lambda}_{i+1,j+1}(\omega - \omega_i)(P - P_j)]\end{aligned} \tag{29}$$

$$\Delta\omega_i = \omega_{i+1} - \omega_i,$$
$$\Delta P_j = P_{j+1} - P_j. \tag{30}$$

Fig. 6 shows an experimentally-determined optimal-flux mesh over a speed range of 2000–5000 r/min and a torque range of 4–20 N·m. Machine efficiencies, calculated using the expression

$$\text{eff}_{\text{machine}} = 1 - \frac{P_{\text{mot}} + P_{\text{gen}}}{2P_{\text{mot}}} \tag{31}$$

where P_{mot} and P_{gen} are the average powers entering the motor and generator, respectively, are presented in Fig. 7. These average power levels were calculated from voltage and current measurements made at the machine terminals.

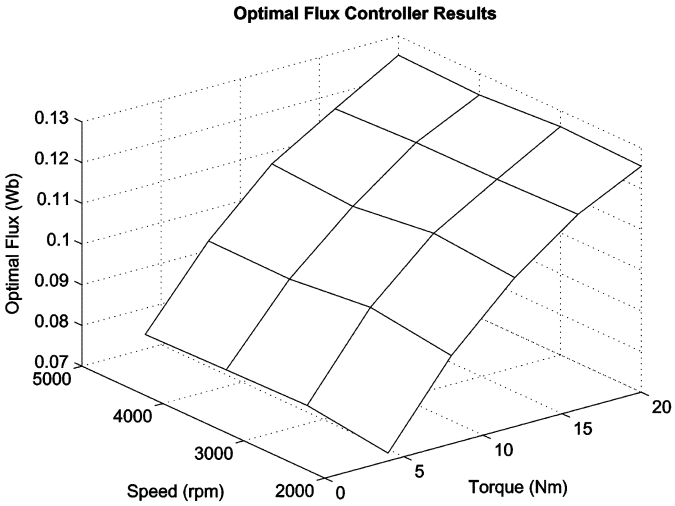

Fig. 6. Experimentally determined optimal flux mesh.

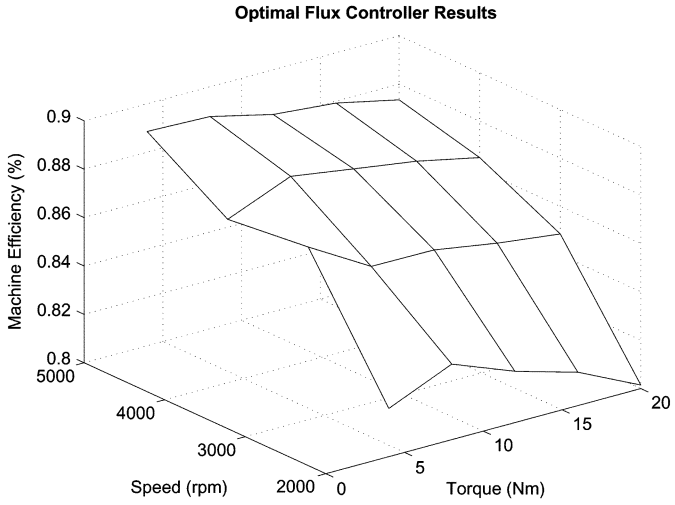

Fig. 7. Optimized machine efficiencies.

The experimental efficiencies increase with speed, as is expected at low speeds since power output increases linearly with speed for a given torque output yet losses, which are predominantly copper losses, remain relatively constant. The efficiencies also decrease slightly with increasing torque. This effect is likely caused by magnetic saturation of the machine at high flux levels, or by core losses that increase more quickly than the square of the flux linkage. Saturation of the machine reduces the effective saliency of the rotor, and hence reduces performance.

VII. Conclusion

A position-sensorless stator-flux-oriented controller for synchronous reluctance machines has been presented and verified through experimental results. Further, an experimental technique for determining operating points for this controller with minimal losses was presented.

Appendix A
Synchronous Reluctance Torque Derivation

Torque in a synchronous reluctance machine can be determined by differentiating co-energy $W'(\mathbf{i}', \theta_r)$ [1]

$$\begin{aligned} W'(\mathbf{i}', \theta_r) &= \frac{3}{4}\mathbf{i}'^T\mathbf{L}(\theta_r)\mathbf{i}' \\ \tau_e &= \frac{\partial W'(\mathbf{i}', \theta_r)}{\partial \theta_r} \\ &= \frac{3P}{4}\mathbf{i}'^T e^{\mathbf{J}P\theta_r}(\mathbf{JL} - \mathbf{LJ})e^{-\mathbf{J}P\theta_r}\mathbf{i}' \\ &= \frac{3P}{2}\mathbf{i}'^T\mathbf{JL}(\theta_r)\mathbf{i}' \\ &= \frac{3P}{2}\mathbf{i}'^T\mathbf{J}\lambda \\ &\approx \frac{3P}{2}(\mathbf{i} - G_c\mathbf{v})^T\mathbf{J}\lambda. \end{aligned} \tag{32}$$

In deriving (32) we have made use of the relations

$$\mathbf{A}e^{\mathbf{Ax}} = e^{\mathbf{Ax}}\mathbf{A} \tag{33}$$

and

$$\mathbf{x}^T\mathbf{Ax} = \frac{1}{2}(\mathbf{x}^T\mathbf{Ax} + \mathbf{x}^T\mathbf{A}^T\mathbf{x}). \tag{34}$$

Appendix B
Quadrature Current Transfer Function Derivation

The system to be linearized is given below

$$\begin{aligned} \frac{d}{dt}\theta_s &= \frac{v_q^\lambda - Ri_q^\lambda}{||\lambda||} - P\omega_r = \frac{\bar{v}_q^\lambda}{||\lambda||} - P\omega_r \\ &= f\left(\bar{v}_q^\lambda, ||\lambda||, \omega_r\right) \\ i_q^\lambda &= [1 \quad 0]e^{\mathbf{J}\theta_s}\mathbf{L}^{-1}e^{-\mathbf{J}\theta_s}\begin{bmatrix} ||\lambda|| \\ 0 \end{bmatrix} \\ &= h(\theta_s, ||\lambda||). \end{aligned} \tag{35}$$

The linearized system is then given by

$$\begin{aligned} \frac{d}{dt}\theta_s &= a\theta_s + b\bar{v}_q^\lambda \\ i_q^\lambda &= c\theta_s \end{aligned} \tag{36}$$

where

$$\begin{aligned} a &= \frac{\partial f\left(\bar{v}_q^\lambda, ||\lambda||, \omega_r\right)}{\partial \theta_s} = 0 \\ b &= \frac{\partial f\left(\bar{v}_q^\lambda, ||\lambda||, \omega_r\right)}{\partial \bar{v}_q^\lambda} = \frac{1}{||\lambda||} \\ c &= \frac{\partial h(\theta_s, ||\lambda||)}{\partial \theta_s} \\ &= [1 \quad 0]e^{\mathbf{J}\theta_s}(\mathbf{JL}^{-1} - \mathbf{L}^{-1}\mathbf{J})e^{-\mathbf{J}\theta_s}\begin{bmatrix} ||\lambda|| \\ 0 \end{bmatrix} \\ &= \left(\frac{1}{L_q} - \frac{1}{L_d}\right)(\cos^2(\theta_s) - \sin^2(\theta_s))||\lambda||. \end{aligned} \tag{37}$$

That said, the transfer function $(I_q^\lambda(s)/\bar{V}_q^\lambda(s))$ is as follows:

$$\frac{I_q^\lambda(s)}{\bar{V}_q^\lambda(s)} = c(s-a)^{-1}b = \frac{1}{s}\left(\frac{1}{L_q}-\frac{1}{L_d}\right)(\cos^2(\theta_s)-\sin^2(\theta_s)). \quad (38)$$

REFERENCES

[1] A. E. Fitzgerald Jr., C. Kingsley, and S. D. Umans, *Electric Machinery*. New York: McGraw-Hill, 1990.

[2] J. E. Fletcher, B. W. Williams, and T. C. Green, "Efficiency aspects of vector control applied to synchronous reluctance motors," in *Conf. Rec. IEEE-IAS Annu. Meeting*, vol. 1, Oct. 1995, pp. 294–300.

[3] T. Fukao, A. Chiba, and M. Matsui, "Test results on a super-high-speed amorphous-iron reluctance motor," *IEEE Trans. Ind. Applicat.*, vol. 25, pp. 119–125, Jan./Feb. 1989.

[4] H. Hofmann and S. R. Sanders, "High speed synchronous reluctance with minimized rotor losses," *IEEE Trans. Ind. Applicat.*, vol. 36, pp. 531–539, Mar./Apr. 2000.

[5] S. J. Kang and S. K. Sul, "Efficiency optimized vector control of synchronous reluctance motor," in *Conf. Rec. IEEE-IAS Annu. Meeting*, vol. 1, Oct. 1996, pp. 117–121.

[6] J. Kowalik and M. R. Osborne, *Methods for Unconstrained Optimization*. New York: Elsevier, 1968.

[7] R. Lagerquist, I. Boldea, and T. J. E. Miller, "Sensorless control of the synchronous reluctance motor," in *Conf. Rec. IEEE-IAS Annu. Meeting*, vol. 1, Oct. 1993, pp. 427–436.

[8] J. H. Lee, D. S. Hyun, J. C. Kim, and D. M. Lee, "Iron core loss minimization scheme on vector control for the synchronous reluctance motor," in *Conf. Rec. IEEE-IAS Annu. Meeting*, vol. 1, Oct. 1998, pp. 677–684.

[9] T. A. Lipo, A. Vagati, L. Malesani, and T. Fukao, "Synchronous reluctance motors and drives—A new alternative," presented at the 26th IEEE-IAS Annu. Meeting, Houston, TX, 1992.

[10] T. Matsuo, A. El-Antably, and T. A. Lipo, "A new control strategy for optimum efficiency operation of a synchronous reluctance motor," in *Conf. Rec. IEEE-IAS Annu. Meeting*, vol. 1, Oct. 1996, pp. 109–116.

[11] T. Matsuo and T. A. Lipo, "Field-oriented control of synchronous reluctance machine," in *Proc. IEEE PESC'93*, June 1993, pp. 425–431.

[12] E. Polak, *Optimization: Algorithms and Consistent Approximations*. Berlin, Germany: Springer-Verlag, 1997.

[13] T. Senjyu, A. Omoda, and K. Uezato, "High efficiency control of synchronous reluctance motors using extended kalman filter," in *Proc. IEEE PESC'98*, vol. 2, May 1998, pp. 1309–1314.

[14] Y. Tomori, T. Senjyu, and K. Uezato, "Vector control of synchronous reluctance motors including stator-iron loss with on-line parameter measurement," in *Proc. IEEE PESC'94*, vol. 1, June 1994, pp. 508–513.

[15] A. Vagati, "The synchronous reluctance solution: A new alternative in ac drives," in *Proc. 20th Int. Conf. Industrial Electronics, Control, and Instrumentation*, vol. 1, Sept. 1994, pp. 1–13.

[16] L. Xu and J. Yao, "A compensated vector control scheme of a synchronous reluctance motor including saturation and iron losses," in *Conf. Rec. IEEE-IAS Annu. Meeting*, vol. 1, Sept. 1991, pp. 298–304.

Heath F. Hofmann (M'90) received the B.S. degree from the University of Texas, Austin, in 1992, and the M.S. and Ph.D. degrees from the University of California, Berkeley, in 1997 and 1998, respectively, all in electrical engineering.

He recently began his career at The Pennsylvania State University, University Park, as an Assistant Professor in the Department of Electrical Engineering. His research interests are in power electronics and electromechanical systems. Specific interests are the development and application of sensorless field-oriented control schemes, quiet electric drives, high-speed machine design, piezoelectric power generation, and the application of advanced numerical methods to the design and simulation of electromechanical systems, focusing on finite-element analysis techniques. He is the primary coauthor on several journal papers on electric machine design and control.

Dr. Hofmann received the Prize Paper Award from the Electric Machines Committee at the 1998 Annual Meeting of the IEEE Industry Applications Society.

Seth R. Sanders (M'88) received S.B. degrees in electrical engineering and physics in 1981 and the S.M. and Ph.D. degrees in electrical engineering in 1985 and 1989, respectively, from Massachusetts Institute of Technology (MIT), Cambridge.

He was a Design Engineer with the Honeywell Test Instruments Division, Denver, CO. Since 1989, he has been a member of the faculty of the Department of Electrical Engineering and Computer Sciences, University of California, Berkeley, where he is presently a Professor. His research interests are in high-frequency power conversion circuits and components, in design and control of electric machine systems, and in nonlinear circuit and system theory as related to the power electronics field. He is presently actively supervising research projects in the areas of flywheel energy storage, novel electric machine design, renewable energy, and digital pulsewidth-modulation strategies and associated IC designs for power conversion applications. During the 1992–1993 academic year, he was on industrial leave with National Semiconductor, Santa Clara, CA.

Prof. Sanders was a recipient of the NSF Young Investigator Award in 1993. He has served as Chair of the IEEE Technical Committee on Computers in Power Electronics, and as a Member-At-Large of the IEEE Power Electronics Society AdCom. He is a coauthor of papers awarded prizes by the IEEE Power Electronics and IEEE Industry Applications Societies.

Ahmed EL-Antably (M'02) received the M.S. degree in control engineering and the Ph.D. degree in electrical engineering from the University of Sussex, Brighton, U.K., in 1975 and 1980, respectively.

Currently, he is with Allison Transmission, Indianapolis, IN. He worked in various oil fields pumping stations from 1968 to 1973. He was also with Westinghouse Electric Corporation from 1980 to 1989, involved in the design, analysis, manufacturing, testing, and service of electric drive motor systems. He is the author of 15 publications and the holder of four patents.